A 3D mathematical model for sprouting angiogenesis

a semi-stochastic cell based formalism

F.D. (Frans) Bookholt

Delft University of Technology

TU Delft Delft University of Technology

Challenge the future

A 3D MATHEMATICAL MODEL FOR SPROUTING ANGIOGENESIS

A SEMI-STOCHASTIC CELL BASED FORMALISM

by

F.D. (Frans) Bookholt

in partial fulfillment of the requirements for the degree of

Master of Science
in Applied Mathematics

at the Delft University of Technology,
to be defended publicly on Monday September 1, 2014 at 10:00 AM.

Supervisor:	Dr. ir. F.J. Vermolen	
Thesis committee:	Dr. ir. F.J. Vermolen	Delft University of Technology
	Prof. dr. ir. C. Vuik,	Delft University of Technology

This thesis is confidential and cannot be made public until January 1, 2015.

TU Delft Delft University of Technology

CONTENTS

NOMENCLATURE

ATECs Adipose Tissue Endothelial Cells - Endothelial cells derived from fat tissue, mostly from adipose human subjects.

bFGF basic Fibroblast Growth Factor - An angiogenic growth factor secreted by fibroblasts.

BM Basement Membrane or Boundary Membrane. A fibre like structure underneath ECs

CPM Cellular Potts model

ECF Extracellular Fluid

ECM Extracellular Matrix - The mixture of proteins, growth-factors and carbohydrates surrounding cells *in vivo*

ECs Endothelial Cells

HDVECs Human Dermal Vascular Endothelial Cells - ECs derived from the human dermis.

MDGFs Macrophage Derived Growth Factors

MMP Matrix metalloproteinases - A group of proteases degrading the basement membrane

PDE Partial Differential Equation

TNF-α Tumor Necrosis Factor alpha - A cytokine secreted by a variety of cells and adipose tissue.

TST Tissue Simulation Toolbox

uPA urokinase-type Plasminogen Activator - Protease degrading fibrin.

VE-cadherin Vascular Endothelial Cadherin

VEGF Vascular Endothelial Growth Factor

1

ANGIOGENESIS

1.1. INTRODUCTION

Angiogenesis is the biological mechanism by which new blood vessels sprout from existing ones. It differs from vasculogenesis, which is the *de novo* growth of the primary vascular network from initially dispersed endothelial cells (ECs). Vasculogenesis is predominant in embryonic tissue whilst new vasculature in the adult body arises mostly from angiogenesis. ECs, lining the inside of blood vessels, react to different angiogenic stimuli and inhibitors. Among the stimuli is the vascular endothelial growth factor (VEGF) which is up-regulated in tissue where the vascular structure is damaged or insufficiently developed to meet oxygen demand.

The identification of the processes involved in angiogenesis is quite recent and has stirred increased interest in therapeutic applications [1]. One can think of tissue repair in wound beds, inhibition of growth of tumorous tissue or vascular reform during the female reproductive cycle. Rossiter et al. [2] showed that VEGF induced angiogenesis is crucial for wound healing in an experiment where wounds were inflicted upon normal and VEGF-deficient mice. New vasculature ensures supply of oxygen and lymphocytes and disposal of carbon dioxide and lactates, acceleration wound healing and tissue reconstruction. The increased creation of new vasculature around tumorous tissue is believed to follow the same process and inhibiting angiogenesis is therefore an important topic in clinical cancer research.

Biochemical experiments can be either hard, time consuming, expensive or unethical. Computational models can be used to provide an easy, quick and cheap way to get insights that are hard to obtain otherwise without conducting a laboratory experiment. Computer simulation will never make lab experiments obsolete but can provide guidance in targeting viable hypotheses before conducting real-life experiments. Mathematical modeling of biological cellular processes dates back to the simulation by Glazier and Graner in 1992. They describe natural sorting behavior of different cell types [3] and different re-arrangement patterns driven by the differential adhesion hypothesis [4]. This hypothesis states that cells of different types have specific potential energies upon adhesion, driving sorting behavior.

In these simulations, the cellular Potts model[1] (CPM) is used. A CPM for vasculogenesis based on this work was made by Merks et al. [5],[6] in which a layer of partial differential equations (PDE's) models the chemoattractants. Later, Merks added Vascular Endothelial cadherin (VE-cadherin) caused contact-inhibited chemotaxis to simulate angiogenic-like structure formation [7]. From an initial clump of ECs in the model sprouting behavior appears. Merks postulates that both vasculogenesis and angiogenesis must be driven by the same principles. To produce these results, a generic library called the Tissue Simulation Toolkit (TST) was written in C++ starting from 2004 modeling the CPM described by Glazier et al. [4] in a generic way. Merks [7] extensively describes the advantages of a cell based approach over a continuum approach. However, his CPM is computationally heavy, limiting the scalability of the possible problem domain.

[1] Also sometimes referred to as the large-Q Potts model or Glazier-Graner-Hogeweg model.

Vermolen and Gefen [8] have described tissue behavior using a semi-stochastic cell-based formalism to model the migration of cells in colonies in the context of wound healing, tumor growth, bone ingrowth and contraction formation. Movement of cells is assumed to be the result of a strain energy density working as a mechanical stimulus. The model tracks displacement and viability of individual spherical cells.

The aim of this research is to apply this semi-stochastic cell-based formalism to describe angiogenesis, hence connecting this modeling approach with the subject of Merks' work. The need for such a model is clearly stated in the discussion of Vermolen's work [9]. Thanks to the computational less heavy character compared to the CPM, we hope to be able to simulate larger areas to get a better glance at large scale behavior whilst still being able to benefit from the cell-based character of the model. We also make improvements to the biochemical model for the substrate. The challenge will be to to transport the advantages of Merks' CPM, like cell shape specific behavior, tracking of elongation patterns and cell-cell contact behavior, to this new formalism.

To biochemically verify our results, we work together with the VU Medical Center Dermatology Department. This department does *in vitro* laboratory research on many dermal cell types and dermal processes, among which ECs, angiogenesis and its growth factors. The first aim of this research is to mimic their *in vitro* work using our computational model, simulating the angiogenic response to different chemical stimuli like VEGF.

1.2. ANGIOGENESIS

1.2.1. IN VIVO ANGIOGENESIS

Sprouting angiogenesis is the formation of new blood vessels from existing ones, usually towards hypoxic tissue to meet oxygen demand. In sprouting angiogenesis new microvascular structures "sprout" from existing blood vessels. The process can be roughly divided in five phases depicted in Figure 1.1. Firstly, angiogenic growth factors, like VEGF, are secreted by oxygen deprived cells. ECs in existing vessels get activated to form new vasculature and a selected number of ECs differentiate in tip cells which lead the sprout. The tip cells release proteases, among others matrix metalloproteinases (MMP) , which degrade the basement membrane underneath the endothelium. The ECs than migrate into the surroundings, forming sprouts by degrading the extracellular matrix (ECM) by proteases like the urokinase-type plasminogen activator (uPA) . In the morphogenesis phase, by the lack of VEGF, the sprouting stabilizes and new boundary membrane is formed around the formed vasculature. Sprouting occurs at a rate of several millimeters per day.

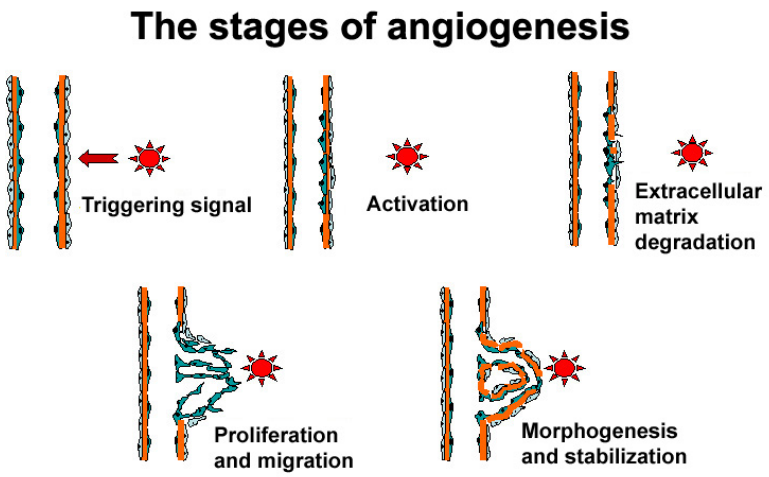

Figure 1.1: Phases of sprouting angiogenesis

In intussusceptive angiogenesis, also splitting angiogenesis, ECs in an existing vessel connect to form two lumen, splitting an existing vessel into two vessels. This type of angiogenesis is not considered in this research.

1.2.2. EXPERIMENTAL SPROUTING ASSAY SETUP

The dermatology department of the VU University Amsterdam Medical Center carries out several *in vitro* assays using either Adipose Tissue Endothelial Cells (ATECs) or Human Dermal Vascular Endothelial Cells

(HDVECs) on different substrates like fibrin or gelatin gels. We are particularly interested in the sprouting assay on fibrin gel which is carried out in a standard 96 well plate depicted in Figure 1.2.

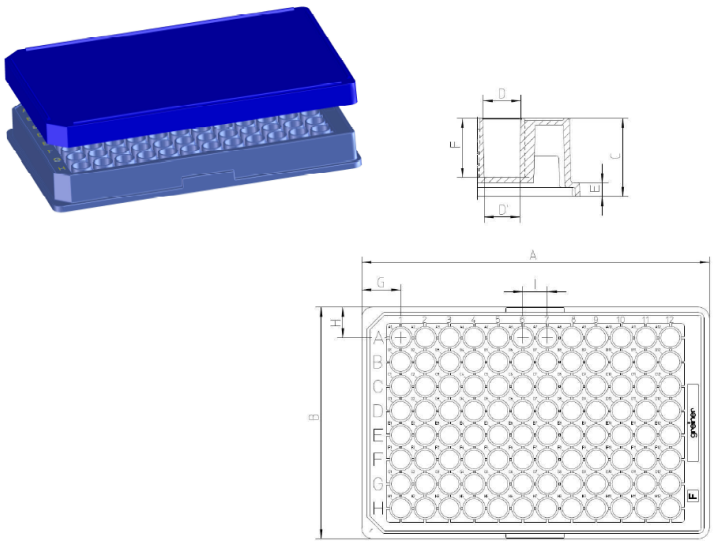

Figure 1.2: 96 well plate. Wells are cylindrical with a diameter of 7 mm

On the first day, a 100 μl fibrin gel (3 mg/ml fibrinogen with 0.5 μg/ml thrombine IIa) is placed in each well on top of which a 100 μl solution is poured containing around 20.000 EC's. This entails a total height of the fibrin and fluid in the well of 5.2 mm. Experimental observations show that typical EC's have a diameter of around 45 μm. The EC's "sink" and adhere to the gel, thus forming a confluent mono layer covering almost the complete surface of the fibrin as depicted in the microscopic images in Figure 1.3.

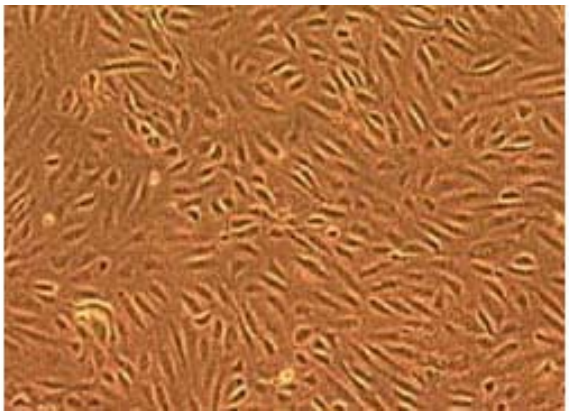

Figure 1.3: HDVEC type ECs on a fibrin gel.

On the second day, a 2 ng/ml Tumor Necrosis Factor alpha (TNF-α) concentration is added and either different concentrations VEGF or basic Fibroblast Growth Factor (bFGF) . TNF-α is a cytokine, *in vivo* secreted by adipose tissue, that is added to activate the EC's. The effect of both angiogenic stimuli VEGF and bFGF is measured for different concentrations. VEGF is added in concentrations $25ng/ml$, $10ng/ml$, $3{,}3ng/ml$, $1{,}1ng/ml$, $0{,}3ng/ml$ and $0{,}1ng/ml$. bFGF is added in concentrations $10ng/ml$, $3{,}3ng/ml$, $1{,}1ng/ml$, $0{,}3ng/ml$ and $0{,}1ng/ml$.

On either the fourth or fifth day, dependent on the donor specific cell motility, the substrates are fixated. The sprouting into the fibrin gel is observed using microscopic images.

1.2.3. DRIVING FORCES ON CELLS IN SPROUTING ANGIOGENESIS

We identify several factors driving the motility of cells on the fibrin matrix. To what extent each process is of influence or even dominant is a topic of future research.

CHEMOTAXIS

Gamba [10] and Serini [11] describe chemotaxis as the movement of cells in response to a chemical stimulus. One speaks of positive (negative) chemotaxis if the movement is in the (opposite) direction of the gradient and the chemical is called a chemoattractant (chemorepellent). Chemoattractants may be, following the Keller-Segel model formulated by Horstman [12], secreted by the cells themselves, thus forming isolated clusters of cells. The chemotactic process is thanks to pseudopodia on the cell membranes "reaching" towards higher concentrations of the chemoattractant and pulling the cell in this direction. Inflammatory mediators such as TNF-α may increase the motility of cells.

HAPTOTAXIS

Cells "pull" on the ECM causing a strain by which other cells get pulled along the stress lines. As of 1995, mathematical models for haptotaxis have been proposes by Vernon [13], Namy [14] and Manoussaki [15, 16].

1.2.4. CONTACT FORCES

Cells can adhere to each other by physically attaching their cell membranes using surface proteins like cadherins. ECs adhere to each other using Vascular Endothelial cadherin (VE-cadherin) bounds. VE-cadherin at the same time works as in inhibitor of chemotactic movement caused by VEGF by binding to the same receptor needed for chemotaxis. Merks describes this contact inhibition in his CPM in [17].

Cells also adhere to the ECM using transmembrane integrin receptors. This causes resistance in movement caused by external forces.

ELASTICITY

ECs have an optimal, elliptic, shape and exercise forces on elastic deformation. Gefen [18] proposes a model for these forces.

1.3. MODELING ANGIOGENESIS MATHEMATICALLY

In this section we explore the different methods of modeling angiogenesis mathematically. We distinguish CPMs, Semi stochastic cell-based models and continuum models and compare them. It is important to note that all models use PDEs to model the diffusion, reaction and production of chemoattractants and other chemicals. The difference lies in the way the models describe cell behavior. The CPM models individual cells as collections of lattice sites. The semi-stochastic cell based model proposes that individual cells are spheres. Continuum models describes cell densities and therefore do not track movement of individual cells.

1.3.1. THE CELLULAR POTTS MODEL

The CPM for simulation of biological cells was first used by Glazier and Graner in 1992 [3]. It is a lattice-based computational model derived from cellular-automaton models having stochastic evolvement. It assigns a cell ID $\sigma = 1,\dots,N$ (formerly "spin") to a region of lattice sites. Lattice sites having the same ID form N biological cell. The model evolves by updating the lattice-sites one at a time according to probabilistic rules and a Hamiltonian function $\mathcal{H}$ assigning an effective energy to each lattice-site.

At each step, a lattice site σ is picked randomly and immediately it's cell ID i is changed to j whenever the effective energy gain $\Delta\mathcal{H} = \mathcal{H}(\sigma_j) - \mathcal{H}(\sigma_i)$ is negative (i.e. more energy efficient) and it is changed with a probability whenever the gain is positive, i.e.

$$\mathbb{P}(\Delta\mathcal{H}) = \begin{cases} 1 & \text{if} \Delta\mathcal{H} < 0, \\ e^{\frac{-\Delta\mathcal{H}}{kT}} & \text{if} \Delta\mathcal{H} \geq 0. \end{cases}$$

Here, T is the temperature and k is a parameter governing the likelihood of energy inefficient changes. Cell ID changes are only allowed to cell IDs of the adjacent lattice sites.

The Hamiltonian plays a central role in the proliferation of the cells. Glazier and Graner [3] implemented a Hamiltonian incorporating cell-cell adhesion, connectivity of the cells, elasticity (shape constraint) and target volume. In the model by Merks [6], we see the Hamiltonian

$$\begin{aligned} H =& H_{contact} + H_{shape} + H_{haptotaxis} \\ =& \sum_{x,x'} J_{\tau(x),\tau(x')} \\ &+ \sum_{c \in cells} \lambda_{area}(\tau_c)[A(c) - A_{target}(\tau_c)]^2 + \lambda_{perimiter}(\tau_c)[P(c) - P_{target}(\tau - c)]^2 \\ &+ \lambda_{haptotaxis}(c(x') - c(x)), \end{aligned}$$

where x represents the current lattice site and x' represent the adjacent lattice sites. τ represents the cell ID. The λ's are scaling parameters to divide priority in the Hamiltonian between the different effects and A_{target} and P_{target} are the desired cell area and perimeter.

A year later, Glazier and Graner added chemotaxis, the movement of cells in the direction of a gradient of a chemoattractant c [4]. The chemotaxis in their model is based on a chemical gradient described by the PDE (following their notation)

$$\frac{\partial c}{\partial t} = \alpha \delta_{\sigma(x),0} - (1 - \delta_{\sigma(x),0})\epsilon c + \nabla^2 c,$$

solved by a finite difference scheme on a lattice coinciding with the CPM lattice. Here, $\delta_{\sigma(x),0}$ is 1 inside cells and 0 outside. α and ϵ are sourcing and reaction constants.

Although not necessarily shaped like this, CPMs mostly have a fixed square lattice. This can lead to coarse shapes, especially for cells containing few lattice sites. The recursive lattice updates can be computationally heavy. In older applications, the sequential modified Metropolis algorithm described by Chen [19] is used. In 2007 Chen et al. introduced a parallel algorithm using checkerboard subgrids to speed up computations. This allows for simulations with up to 10^7 lattice sites.

Merks claims that the CPM is beneficial in describing cell phenomenology like shape, elongation and cell-cell contact interaction compared to continuum models. Furthermore he claims the model to be advantages in describing how collections of exhibiting a certain phenomenology interact during biological morphogenesis [5]. The TST was used to study the effects of cell elongation on vasculogenesis [6] and Merks conclude that cell shape and cell-cell contact interaction are key in the process of angiogenesis.

1.3.2. SEMI-STOCHASTIC CELL-BASED MODEL

Vermolen and Gefen have formulated a semi-stochastic cell-based formalism for migration of cells in colonies in [8]. In their work on a substrate $\Omega \subset \mathbb{R}^2$, a set of N hemispherical cells is modeled. The choice for spherical cells is for computational reasons. For an overview of possibilities to include cell shape changes induces by chemotaxis or mechanical influences, we refer the reader to [20]. They model four different types of cell motility: haptotaxis, proliferation, random movement and elastic contact movement. Chemotaxis is not yet implemented in this model, so we will consider this as an addition in upcoming work. We consider these separately.

HAPTOTAXIS

The haptotactic response of cells to strain in the matrix is caused by the effect of traction forces of the cells themselves. We first encounter this concept in a continuum model by Manoussaki in 1996 [15] and 2003 in [16]. By this traction force, the substrate is distorted around the cell. This distortion is felt by other cells, which distort the substrate as well by applying their own upward pulling forces. Individual cells sense the distortion field through the strain energy density and then move along the stress lines. Vermolen and Gefen [8] state that the strain energy density caused by an individual cell i, following Hooke's law, is maximal at the cell center $\mathbf{r}_i$

$$M_i^0 = \frac{F_i^2}{2\pi^2 E_s(\mathbf{r}_i) R^4},$$

where F_i is the maximal traction force of cell i, $E_s(_i)$ is the local elasticity modulus of the substrate and R is the cell radius. Furthermore, they approximate, according to the findings by Merkel in [21], that the strain energy density decays exponentially with the radius with a rate proportional tot the ratio λ_i of the elasticity modulus of the substrate $E_s(\mathbf{r}_i)$ at the cell center $\mathbf{r}_i$ and the elasticity modulus E_i of the cell itself, i.e.

$$M_i(\mathbf{r}) = M_i^0 \exp\left(-\lambda_i \frac{\|\mathbf{r}-\mathbf{r}_i\|}{R}\right) = M_i^0 \exp\left(-\frac{E_s(\mathbf{r}_i)}{E_i}\frac{\|\mathbf{r}-\mathbf{r}_i\|}{R}\right). \tag{1.1}$$

Then they argue that the total strain energy density is the sum of the strain energies of the individual cells and evaluate the total strain energy density at a cell center $\mathbf{r}_i$ to be

$$M(\mathbf{r}_i) = M_i^0 + \sum_{j=1_{j\neq i}}^{N} M_j^0 \exp\left(-\frac{E_s(\mathbf{r}_j)}{E_j}\frac{\|\mathbf{r}_i-\mathbf{r}_j\|}{R}\right).$$

Now consider the displacement of a cell by means of the sensed mechanical stimulus. The displacement of cell i caused by cell j is proportional to the strain energy density caused by cell j at cell center $\mathbf{r}_i$, i.e. $M_j(\mathbf{r}_i)$ and in the direction of the line segment connecting cells i to j, i.e. $\mathbf{v}_{ij} = \frac{\mathbf{r}_i-\mathbf{r}_j}{\|\mathbf{r}_i-\mathbf{r}_j\|}$. Vermolen and Gefen argue that the total displacement of cell i is parallel to the sum of the directional displacements z_i caused by all other cells, i.e.

$$\mathbf{z}_i = \sum_{j=1_{j\neq i}}^{N} M_j(\mathbf{r}_i)\mathbf{v}_{ij} = \sum_{j=1_{j\neq i}}^{N} M_j^0 \exp\left(-\frac{E_s(\mathbf{r}_j)}{E_j}\frac{\|\mathbf{r}_i-\mathbf{r}_j\|}{R}\right)\frac{\mathbf{r}_i-\mathbf{r}_j}{\|\mathbf{r}_i-\mathbf{r}_j\|}.$$

One can normalize the direction of the total displacement $\hat{\mathbf{z}}_i = \frac{\mathbf{z}_i}{\|\mathbf{z}_i\|}$. The displacement over time is proportional to the strength of the mechanical signal and we have

$$\begin{aligned}\frac{\mathbf{r}_i(t+\Delta t)-\mathbf{r}_i(t)}{\Delta t} &= \alpha_i M(\mathbf{r}_i(t))\hat{\mathbf{z}}_i,\\ \mathbf{r}_i(t+\Delta t) &= \mathbf{r}_i(t) + \Delta t\alpha_i M(\mathbf{r}_i(t))\hat{\mathbf{z}}_i,\end{aligned}$$

where α_i is a parameter with dimension $\left[\frac{m^3}{Ns}\right]$ in which the force is directed along the substrate, perpendicular to the upward force F. Finally, Gefen [18] argues that this quantity for viable cells equals

$$\alpha_i = \frac{\beta_i R^3}{\mu F_i},$$

where β_i quantifies the mobility of the cell surface of a cell and μ is a dimensionless quantity experimentally tested to be 0.2 [18]. Especially for cells far away from each other, the strain energy $M_j(\mathbf{r}_i)$ can attain very small values, nullifying the contribution to $\mathbf{z}_i$. This advocates a *detection threshold* ϵ for the strain energy density as a minimal signal strength that a cell can detect to reduce computational complexity. For details we refer to Vermolen in [8].

In an additional paper, Vermolen and Gefen [22] add inertia to the movement of the cells and a slowing parameter depending on the lactate concentration in infected wound tissue. The concentration of the lactate is modeled by a PDE where bacteria are added as point sources of lactate.

A topic open to research is how to extend this formalism to the 3 dimensional situation we want to model.

PROLIFERATION

Vermolen and Gefen introduce cell death and proliferation into the model using a stochastic process. At each time step, each cell has a probability of dying, making the cell stationary and invariant of the strain energies. Proliferation is modeled by adding a daughter cell and giving both cells a displacement as the mother cell would have gotten with an extra tangent displacement $\pm R$. Improvements upon this process can be made.

RANDOM MOVEMENT

Vermolen and Gefen add random movement to the cells using a term $\Delta t(1-u_i)\mathbf{w}$ where

$$u_i = u_i(y_i) = \begin{cases} 1, \text{if } y_i \leq p_{mp} \\ 0, \text{if } y_i > p_{mp} \end{cases}$$

for $Y_i \sim U(0,1)$ and some parameter p_{mp} and $\mathbf{w}$ is a unit vector with stochastic angle.

In further research, we will use a different approach by adding a 3 dimensional Wiener process $\mathbf{W}_t = [W_t^1, W_t^2, W_t^3]^T$ having $\mathbf{W}_0 = 0$, $t \rightarrow \mathbf{W}_t$ continuous a.e. and for $0 \leq s \leq t$ having $W_t^i - W_s^i \sim N(0, t-s)$ for $i = 1,2,3$.

ELASTIC CONTACT MOVEMENT

Cells impinging upon each other will exercise repulsive forces. The direction of the force is along the line segment connecting the cell centers and the magnitude is, according to elastic contact mechanics described in [18], depending on the depth h both cells have to dent due to the collision. Using arguments from contact mechanics from Johnson [23], Gefen describes the strain energy M^{ij} due to a collision between cells i and j to be

$$M^{ij} = \frac{4}{15\sqrt{2}} \frac{E}{\pi} \left(\frac{h}{R} \right)^{5/2}$$

in which again R is the cell radius and E_j is the elastic modulus. Since the contact forces are always in the opposite direction of the haptotactic forces, Vermolen subtracts this strain energy from the strain energy density caused by the haptotactic cell forces in Equation 1.1, i.e. $\tilde{M}_i(\mathbf{r}) = M_i(\mathbf{r}) - M^{ij}$ and use $\tilde{M}_i(\mathbf{r})$ in Equation **??**.

CHEMOTAXIS

As with the CPM, chemicals in the tissue are modeled by PDE's. Chemotaxis is not yet implemented in this method but can be modeled by imposing forces on cells proportional to and in the direction of the chemical gradient. This still is work for future research.

An alternative approach for modeling the chemicals is to model cells as point sources and use Greens functions of the PDE's to model the impulse response. We choose not to implement this approach.

1.3.3. CONTINUUM MODELING

To finalize our investigation of biological models in the field of angiogenesis, we focus on a large number of continuum models consisting of systems of PDE's. Alarcon and Chaplain [24] give an excellent overview of continuum models up to the year 2005 for tumor induced angiogenesis as well as a list of advantages and disadvantages of these models. Many early models, like those proposed by Gaffney [25] or Anderson [26] are based on phenomenological arguments or design principles to describe the angiogenic process. Anderson [26] came up with a continuum-discrete model including fibronectin induced haptotaxis as a governing factor. As the research into different angiogenic growth factors progressed, models following a more biochemical reasoning appeared like those by Orme [27], Levine [28] and Vermolen [29]. Schugart et al. [30] and Xue et al. [31] both propose elaborate models incorporating multiple cell types (ECs, fibroblasts, Tip cells and inflammatory cells) and different substances (oxygen, VEGF and ECM) in one coupled continuum system to describe oxidative stress and angiogenesis in wound healing. An elaborate continuum model on wound closure incorporating contraction and angiogenesis is proposed by Vermolen and Javierre in [32]. We believe that these models provide the most recent developments in continuum modeling of angiogenesis.

In both types of models, cells are modeled as densities or concentrations. To illustrate this, we briefly consider the model by Gaffney [25] who models concentrations of tip cells n and ECs b incorporating behavior like capillary sprouting, branching, tips joining each other (anastomosis) and tips joining other sprouts. The coupled system derived from a conservation relation is given by

$$\begin{array}{lll} \frac{\partial n}{\partial t} & = - & \frac{\partial J(n)}{dx} + f(n,b), \\ \frac{\partial b}{\partial t} & = -\lambda_5 & \frac{\partial J(n)}{dx} + g(n,b), \end{array}$$

where

$$J(n) = -D_1 \frac{\partial n}{\partial x} - D_2 n \frac{\partial b}{\partial x}$$

is the tip cells' flux,

$$f(n,b) = \lambda_2 n = \lambda_3 n^2 - \lambda_4 nb$$

describes the tip cells' kinetics and

$$g(n,b) = \lambda_2 \nu b(b_0 - b) + \lambda_6 \chi nb(b_1 - b) + \lambda_5(\lambda_3 n^2 + \lambda_4 nb)$$

describes the kinetics of the ECs. The model replaces both haptotactic and chemotactic movement we saw in previous models by a movement in the direction of decreasing blood vessel density. The parameter λ_2 governs tip branching. λ_3 governs the joining of tips to create a circuit and λ_4 governs tips joining the side of a capillary. λ_5 ensures the proportionality between the flux of the tips and the flux of the ECs and is given by the average number of ECs in a capillary sprout. Gaffney uses dimensionless scaling and stationary point analysis to find the dynamics of the system. The parameters are estimated using experimental results. Finally, boundary conditions and initial conditions are formulated and an analytical solution is found using perturbation theory.

Maggelakis [33] proposed a widely used continuum model for angiogenesis in a circular wound bed of radius R in in which capillary tips modeled by a density n act as main source of the oxygen concentration c_O. Oxygen diffuses with a rate D_O, sources from the capillaries at a rate λ_n and is consumed by macrophages at a rate λ_O from some critical oxygen level c_θ at which macrophages appear at the wound site. The macrophages release chemoattractants called Macrophage Derived Growth Factors (MDGFs) denoted by concentration c_m. The MDGFs diffuse at a rate D_m, are produced at a rate λ_m, react within the capillary tips at a rate λ_c and degrade naturally at a rate λ. High concentrations of MDGFs trigger capillary logistic growth up to a certain maximal vascular density L. The system of PDEs describing this process is given by

$$\begin{aligned}
\frac{\partial c_O}{\partial t} &= D_O \nabla^2 c_O + \lambda_n n - \lambda_O \frac{c_O}{c_\theta}, \\
\frac{\partial c_m}{\partial t} &= \begin{cases} D_m \nabla^2 c_m - \lambda c_m + \lambda_m \left(1 - \frac{c_O}{c_\theta}\right), & \text{for } 0 \le r \le R, \\ D_m \nabla^2 c_m - \lambda c_m - \lambda_c \frac{c_m}{c_{\max}}, & \text{for } R < r \le R_{\max}. \end{cases} \\
\frac{\partial n}{\partial t} &= \mu c_m n \left[1 - \frac{n}{L}\right].
\end{aligned}$$

Note that the behavior of the MDGFs is different inside and outside of the wound bed due to the presence of macrophages.

1.3.4. COMPARISON OF THE METHODS

As was expected, all three types of models have their advantages and disadvantages. We discuss their merits and demerits here briefly.

In the CPM, it is easy to track specific cell motility and implement cell shape and size specific behavior as well as cell contact interface specific properties such as contact inhibited chemotaxis. However, the model is computationally heavy and relies on many model choices such as the Hamiltonian function.

The semi-stochastic cell-based model is computationally less heavy but to some extend still benefits from the possibility of tracking cell motility and involvement of contact mechanics. The model is not able to incorporate complicated contact inhibition like the CPM because of the simplified spherical shape of individual cells.

Possibly the main criticism of continuum models of angiogenesis stems from their inability to track individual capillary tips and, hence, to reproduce accurately the patterns of vascular growth. They are however computationally scalable to a very large extent, making them very useful for behavior of tissue on a large scale.

We conclude that the CPM is especially useful to model specific cell behavior on a small scale. The semi-stochastic cell-based model works on a mid-large scale and the continuum models gives the desired results on a large scale where both the CPM and the semi-stochastic cell-based models grow intractable.

2

UPDATING THE CHEMICALS AND THE SUBSTRATE

In this chapter we formulate the differential equations governing the concentrations of the different chemicals and substrate substances over time. We then derive the finite element discretization to approximate the solution. We choose to do so in a 3 dimensional setting to closely mimic the lab work carried out by the dermatology department at the VU University Amsterdam Medical Center. As this literature report was written, this numerical scheme was already implemented in MATLAB.

The formulation of the cell movement is the subject of the next (not yet written) chapter.

2.1. DIFFERENTIAL EQUATIONS GOVERNING THE CHEMICALS IN THE *in vitro* SITUATION - THE SEMI-DISCRETE CELL-BASED CASE

In our semi-discrete cell-based model, we also want to improve the chemical reactions and the composition of the substrate. We therefore model the substrate as fractions BM ρ_B and fibrin ρ_F continuously. We consider the case where both substances can be degraded into Extracellular Fluid (ECF) which fraction is denoted by ρ_E. This entails describing PDE's for the fractions ρ_F, ρ_B and ρ_E too, adding up to 1 (100%). The three equations modeling the substrate fractions must together constitute conservation of mass, i.e. the amount of fibrin and BM degrading must be equal to the gain in mass for the ECM.

We introduce diffusive terms for the four chemicals dependent on the composition of the substrate. For the diffusion of the concentration VEGF c_V we for instance write $D_V = D_V(\rho_F, \rho_B, \rho_E)$. The rate at which the BM degrades under influence of MMP is now proportional to both the fraction of BM and the concentration of MMP c_M, leading to a cross term in the reactive parts of the equations for the concentration MMP and the fraction BM. The same holds for the fibrin fraction ρ_F and the UPa concentration c_U. We then write the concentration VEGF c_V and the concentration DLL-notch c_D. We get the following differential equations:

Chemicals

$$
\begin{aligned}
\text{VEGF} \quad & \frac{\partial c_V}{\partial t} = \nabla\cdot[D_V(\rho_F,\rho_B,\rho_E)\nabla c_V] && - r_V c_V \mathbb{1}_{Tip,Stalk}, \\
\text{DLL-notch} \quad & \frac{\partial c_D}{\partial t} = \nabla\cdot[D_D(\rho_F,\rho_B,\rho_E)\nabla c_D] && - r_D c_D \mathbb{1}_{Stalk} && + s_D \mathbb{1}_{Tip}, \\
\text{UPa} \quad & \frac{\partial c_U}{\partial t} = \nabla\cdot[D_U(\rho_F,\rho_B,\rho_E)\nabla c_U] && - r_U c_U \rho_F && + s_U \mathbb{1}_{Tip}, \\
\text{MMP} \quad & \frac{\partial c_M}{\partial t} = \nabla\cdot[D_M(\rho_F,\rho_B,\rho_E)\nabla c_M] && - r_M c_M \rho_B && + s_M \mathbb{1}_{Tip},
\end{aligned}
$$

Substrates

$$
\begin{aligned}
\text{Fibrin} \quad & \frac{\partial \rho_F}{\partial t} = && - r_F c_U \rho_F, \\
\text{BM} \quad & \frac{\partial \rho_B}{\partial t} = && - r_B c_M \rho_B, \\
\text{ECF} \quad & \frac{\partial \rho_E}{\partial t} = && && + r_F c_U \rho_F + r_B c_M \rho_B.
\end{aligned}
$$

$$
\underbrace{\qquad\qquad}_{Diffusion} \qquad \underbrace{\qquad\qquad}_{Reaction} \qquad \underbrace{\qquad\qquad}_{Sourcing}
$$

2.2. GALERKIN EQUATIONS FOR THE PDE OF c_M

We derive the Galerkin equations for the PDE of only one of these equations. The derivations for the other equations follow the same principles. Consider the PDE on $\Omega \subset \mathbb{R}^3$ for the concentration of MMP c_M where we abbreviate $D_M = D_M(\rho_F,\rho_B,\rho_E)$ to shorten notation:

$$\frac{\partial c_M}{\partial t} = \nabla\cdot[D_M\nabla c_M] - r_M c_M \rho_B + s_M \mathbb{1}_{Tip},$$

with a no-flux boundary condition $\frac{\partial c_M}{\partial n} = 0$ on the boundary Γ.
We multiply by a test function $\varphi \in H^1(\Omega)$ and integrate over Ω:

$$\int_\Omega \frac{\partial c_M}{\partial t}\varphi dV = \int_\Omega \nabla\cdot[D_M\nabla c_M]\varphi dV - \int_\Omega r_M c_M \rho_B \varphi dV + \int_\Omega s_M \mathbb{1}_{Tip}\varphi dV.$$

Using $\nabla\cdot[D_M\nabla c_M]\varphi = \nabla\cdot[D_M)\nabla c_M\varphi] - (\nabla\varphi)\cdot(D_M\nabla c_M)$ and Gauss' divergence theorem we see

$$\int_\Omega \frac{\partial c_M}{\partial t}\varphi dV = \int_\Omega \nabla\cdot[D_M\nabla c_M\varphi]dV - \int_\Omega (\nabla\varphi)\cdot(D_M\nabla c_M)dV - \int_\Omega r_M c_M \rho_B \varphi dV + \int_\Omega s_M \mathbb{1}_{Tip}\varphi dV,$$

and

$$
\begin{aligned}
\int_\Omega \frac{\partial c_M}{\partial t}\varphi dV &= \int_\Gamma [D_M\nabla c_M\varphi]\cdot n d\Gamma - \int_\Omega (\nabla\varphi)\cdot(D_M\nabla c_M)dV - \int_\Omega r_M c_M \rho_B \varphi dV + \int_\Omega s_M \mathbb{1}_{Tip}\varphi dV. \\
&= \int_\Gamma D\frac{\partial c_M}{\partial n}\varphi d\Gamma - \int_\Omega D(\nabla c_M)\cdot(\nabla\varphi)dV - \int_\Omega r_M c_M \rho_B \varphi dV + \int_\Omega s_M \mathbb{1}_{Tip}\varphi dV.
\end{aligned}
$$

Because of the boundary condition, we see that the boundary term drops out and we end up with the weak formulation

$$\int_\Omega \frac{\partial c_M}{\partial t}\varphi dV = -\int_\Omega D_M(\nabla c_M)\cdot(\nabla\varphi)dV - \int_\Omega r_M c_M \rho_B \varphi dV + \int_\Omega s_M \mathbb{1}_{Tip}\varphi dV. \tag{2.1}$$

We introduce a discretization into n_{el} tetrahedral elements with in total n nodal points (nodes). We denote the elements by e_l for $l = 1,\dots,n_{el}$. We denote the nodal points by n_j for $j = 1,\dots,n$ and we denote their spacial coordinates by $\mathbf{x}_j = (x_j,y_j,z_j)^T$. Corresponding with each node n_j we introduce a piecewise linear basis function $\varphi_j = \alpha_j + \beta_j x + \gamma_j y + \delta_j z$. We choose the parameters $\alpha_j,\dots,\delta_j$ (inside each element) such that

on each nodal point n_i we have $\varphi_j = 1$ if $i = j$ and 0 otherwise, so called tent functions. Every element e_l has four nodal points $n_p^{e_l}$ for $p = 1,\dots,4$ and we denote their spacial coordinates by $\mathbf{x}_p^{e_l} = (x_p^{e_l}, y_p^{e_l}, z_p^{e_l})^T$. On each nodal point n_j we introduce a parameter $c_m(n_j)$ which value coincides with the value of the concentration MMP c_M in that point. The parameters c_m form a vector of length n. Note that for the concentration MMP we use c_M with capital M and for the corresponding parameter we use c_m with lower case m. We can now approximate the concentration $c_M \approx \sum_{j=1}^n c_m(n_j)\varphi_j$. To sum up, we define

- elements e_l for $l = 1,\dots,n_{el}$;
- nodes n_j for $j = 1,\dots,n$ having spacial coordinates $\mathbf{x}_j = (x_j, y_j, z_j)^T$;
- basis function $\varphi_j = \alpha_j + \beta_j x + \gamma_j y + \delta_j z$ on a node n_j such that $\varphi_j(\mathbf{x}_i) = 1$ for $i = j$ and 0 otherwise;
- the four vertices $n_p^{e_l}$ of an element e_l for $p = 1,\dots,4$ having spacial coordinates $\mathbf{x}_p^{e_l} = (x_p^{e_l}, y_p^{e_l}, z_p^{e_l})^T$;
- a parameter $c_m(n_j)$ on each node n_j equal to the value of c_M at that nodal point;
- an approximation $c_M \approx \sum_{j=1}^n c_m(n_j)\varphi_j$.

Substituting this approximation into the weak formulation in Equation 2.1 and choosing $\varphi = \varphi_i$ for $i = 1,\dots,n$ we see

$$\int_\Omega \frac{\partial}{\partial t}\left(\sum_{j=1}^n c_m(n_j)\varphi_j\right)\varphi_i dV = -\int_\Omega (\nabla\varphi_i)\cdot(D_M\nabla\left(\sum_{j=1}^n c_m(n_j)\varphi_j\right))dV$$
$$-\int_\Omega r_M\left(\sum_{j=1}^n c_m(n_j)\varphi_j\right)B\varphi_i dV + \int_\Omega S_c \mathbb{1}_{Tip}\varphi_i dV \quad \text{for } i = 1,\dots,n.$$

Changing the order of integration and summation yields a system $M\frac{\partial c_m}{\partial t} + Sc_m = f$ where the matrix elements M_{ij} and S_{ij} and the vector elements f_i are given by

$$\sum_{j=1}^n \underbrace{\int_\Omega \varphi_j\varphi_i dV}_{M_{ij}} \frac{\partial c_m(n_j)}{\partial t} + \sum_{j=1}^n \underbrace{\int_\Omega D_M\nabla\varphi_i\cdot\nabla\varphi_j + r_M\rho_B\varphi_i\varphi_j dV}_{S_{ij}} c_m(n_j) = \underbrace{\int_\Omega s_M\mathbb{1}_{Tip}\varphi_i dV}_{f_i} \quad \text{for } i = 1,\dots,n.$$

We calculate the matrix entries M_{ij} and S_{ij} and the vector elements f_i by splitting up the integrals over all elements, i.e.

$$M_{ij} = \int_\Omega \varphi_j\varphi_i dV = \sum_{l=1}^{n_{el}} \underbrace{\int_{e_l} \varphi_j\varphi_i dV}_{M_{ij}^{e_l}},$$

$$S_{ij} = \int_\Omega D_M\nabla\varphi_i\cdot\nabla\varphi_j + r_M\rho_B\varphi_i\varphi_j dV = \sum_{l=1}^{n_{el}} \underbrace{\int_{e_l} D_M\nabla\varphi_i\cdot\nabla\varphi_j + r_M\rho_B\varphi_i\varphi_j dV}_{S_{ij}^{e_l}},$$

$$f_{ij} = \int_\Omega s_M\mathbb{1}_{Tip}\varphi_i dV = \sum_{l=1}^{n_{el}} \underbrace{\int_{e_l} s_M\mathbb{1}_{Tip}\varphi_i dV}_{f_i^{e_l}}.$$

2.3. THE ELEMENTS MATRICES AND VECTORS FOR DE PDE OF M

We derive approximations for the integrals $M_{ij}^{e_l}$, $S_{ij}^{e_l}$ and $f_i^{e_l}$. For the integrals involving the basis functions, we use the Holand-Bell integration formulas for linear basis functions over simplices proved in [34]. Each element e_l has four corresponding nodes (vertices), denoted by $n_p^{e_l}$ for $p = 1,\dots,4$. If φ_p are linear basis functions on the nodes $n_p^{e_l}$ of the tetrahedral element e_l (simplex in 3d), then we have the exact integral

$$\int_{e_l} (\varphi_1^{e_l})^a (\varphi_2^{e_l})^b (\varphi_3^{e_l})^c (\varphi_4^{e_l})^d \, dV = \|\Delta\|^{e_l} \frac{a!\, b!\, c!\, d!}{(a+b+c+d+3)!}, \tag{2.2}$$

where $\frac{\|\Delta\|^{e_l}}{6}$ is the volume of the element e_l. We calculate $\|\Delta\|$ is calculated by the determinant

$$\|\Delta\|^{e_l} = \begin{vmatrix} 1 & 1 & 1 & 1 \\ x_1^{e_l} & x_2^{e_l} & x_3^{e_l} & x_4^{e_l} \\ y_1^{e_l} & y_2^{e_l} & y_3^{e_l} & y_4^{e_l} \\ z_1^{e_l} & z_2^{e_l} & z_3^{e_l} & z_4^{e_l} \end{vmatrix}.$$

Next, we introduce Newton-Cotes integration for approximation of volume integrals of other than basis functions over a tetrahedron e_l. We see

$$\int_{e_l} f(\mathbf{x}) dV \approxeq \frac{\|\Delta\|^{e_l}}{6} \left(\frac{1}{4} \sum_{p=1}^{4} f(\mathbf{x}_p^{e_l}) \right) = \frac{\|\Delta\|}{24} \sum_{p=1}^{4} f(\mathbf{x}_p^{e_l}), \tag{2.3}$$

where equality holds if $f(\mathbf{x})$ is linear.

We apply Holand-Bell integration (Equation 2.2) to $M_{ij}^{e_l}$. We note that, integrating over e_l, we only have non-zero values for $i, j \in \{n_p^{e_l} | p = 1, \ldots, 4\}$ and this entails

$$M_{ij}^{e_l} = \begin{cases} 0 & \text{for } i, j \notin \{n_p^{e_l} | p = 1, \ldots, 4\}, \\ \frac{\|\Delta\|^{e_l}}{120} & \text{for } i \neq j, \\ \frac{\|\Delta\|^{e_l}}{60} & \text{for } i = j. \end{cases}$$

We now calculate $M_{ij}^{e_l}$ for all combinations $i, j \; in \{n_p^{e_l} | p = 1, \ldots, 4\}$ and we call this M^{e_l}:

$$M^{e_l} = \frac{\|\Delta\|^{e_l}}{120} \begin{bmatrix} 2 & 1 & 1 & 1 \\ 1 & 2 & 1 & 1 \\ 1 & 1 & 2 & 1 \\ 1 & 1 & 1 & 2 \end{bmatrix}.$$

Note that M^{e_l} is an $n \times n$ matrix, but only the rows and columns of the nodes $n_p^{e_l}$ corresponding to element e_l are shown here and the rest of the elements are equal zero.

We approximate $S_{ij}^{e_l}$ by using Newton-Cotes integration (Equation 2.3) and Holand-Bell integration (Equation 2.2). Since the basis function on node i reads $\varphi_i = \alpha_i + \beta_i x + \gamma_i y + \delta_i z$, we see that $\nabla\varphi_i \cdot \nabla\varphi_j = (\beta_i\beta_j + \gamma_i\gamma_j + \delta_i\delta_j)$. Therefore

$$\begin{aligned} S_{ij}^{e_l} &= \int_{e_l} D_M \nabla\varphi_i \cdot \nabla\varphi_j + r_M \rho_B \varphi_i \varphi_j dV, \\ &= \begin{cases} 0 & \text{for } i, j \notin \{n_p^{e_l} | p = 1, \ldots, 4\} \\ (\beta_i\beta_j + \gamma_i\gamma_j + \delta_i\delta_j) \int_{e_l} D_M dV + r_M \int_{e_l} \rho_B \varphi_i \varphi_j dV & \text{for } i, j \in \{n_p^{e_l} | p = 1, \ldots, 4\} \end{cases} \\ &\approx \begin{cases} 0 & \text{for } i, j \notin \{n_p^{e_l} | p = 1, \ldots, 4\} \\ (\beta_i\beta_j + \gamma_i\gamma_j + \delta_i\delta_j) \; \frac{\|\Delta\|^{e_l}}{24} \sum_{p=1}^{4} D_M(\rho_F(\mathbf{x}_p^{e_l}), \rho_B(\mathbf{x}_p^{e_l}), \rho_E(\mathbf{x}_p^{e_l})) & \text{for } i \neq j, \\ (\beta_i^2 + \gamma_i^2 + \delta_i^2) \; \frac{\|\Delta\|^{e_l}}{24} \sum_{p=1}^{4} D_M(\rho_F(\mathbf{x}_p^{e_l}), \rho_B(\mathbf{x}_p^{e_l}), \rho_E(\mathbf{x}_p^{e_l})) + r_M \frac{\|\Delta\|^{e_l}}{24} \rho_B(\mathbf{x}_i^{e_l}) & \text{for } i = j. \end{cases} \end{aligned}$$

Here, by definition of the parameters for the different chemical variables, we have $\rho_F(\mathbf{x}_p^{e_l}) = \rho_f(n_p^{e_l})$, $\rho_B(\mathbf{x}_p^{e_l}) = \rho_b(n_p^{e_l})$ and $\rho_E(\mathbf{x}_p^{e_l}) = \rho_e(n_p^{e_l})$, hence

$$S_{ij}^{e_l} \approx \begin{cases} 0 & \text{for } i, j \notin \{n_p^{e_l} | p = 1, \ldots, 4\} \\ (\beta_i\beta_j + \gamma_i\gamma_j + \delta_i\delta_j) \; \frac{\|\Delta\|^{e_l}}{24} \sum_{p=1}^{4} D_M(\rho_f(n_p^{e_l}), \rho_b(n_p^{e_l}), \rho_e(n_p^{e_l})) & \text{for } i \neq j, \\ (\beta_i^2 + \gamma_i^2 + \delta_i^2) \; \frac{\|\Delta\|^{e_l}}{24} \sum_{p=1}^{4} D_M(\rho_f(n_p^{e_l}), \rho_b(n_p^{e_l}), \rho_e(n_p^{e_l})) + r_M \frac{\|\Delta\|^{e_l}}{24} \rho_b(n_i^{e_l}) & \text{for } i = j. \end{cases}$$

Now, if we define

$$L^{e_l} = \begin{bmatrix} \beta_1^{e_l} & \gamma_1^{e_l} & \delta_1^{e_l} \\ \vdots & \vdots & \vdots \\ \beta_4^{e_l} & \gamma_4^{e_l} & \delta_4^{e_l} \end{bmatrix},$$

then for an element e_l we see that the element matrix becomes

$$S^{e_l} = \frac{\|\Delta\|^{e_l}}{24} \sum_{p=1}^{4} D_M(\rho_f(n_p^{e_l}), \rho_b(n_p^{e_l}), \rho_e(n_p^{e_l})) L^{e_l} (L^{e_l})^T + r_M \frac{\|\Delta\|^{e_l}}{24} \begin{bmatrix} \rho_b(n_1^{e_l}) & & \emptyset \\ & \ddots & \\ \emptyset & & \rho_b(n_4^{e_l}) \end{bmatrix}.$$

The mixed terms $\rho_f(n_p^{e_l}), \rho_b(n_p^{e_l}), \rho_e(n_p^{e_l})$ must be taken explicit care of when we try to implement an implicit time stepping scheme. More on this issue will follow in the time stepping chapter.

By the nature of the basis functions $\varphi_p^{e_l}$ with $p = 1, \ldots, 4$ within an element e_l, we know that they must attain values 1 on their corresponding node p and attain values 0 at all other nodes. If we write $\varphi_p^{e_l} = \alpha_p^{e_l} + \beta_p^{e_l} x + \gamma_p^{e_l} y + \delta_p^{e_l} z$ for $p = 1, \ldots, 4$, we can write these equalities as a system

$$\begin{bmatrix} 1 & x_1^{e_l} & y_1^{e_l} & z_1^{e_l} \\ 1 & x_2^{e_l} & y_2^{e_l} & z_2^{e_l} \\ 1 & x_3^{e_l} & y_3^{e_l} & z_3^{e_l} \\ 1 & x_4^{e_l} & y_4^{e_l} & z_4^{e_l} \end{bmatrix} \begin{bmatrix} \alpha_1^{e_l} & \alpha_2^{e_l} & \alpha_3^{e_l} & \alpha_4^{e_l} \\ \beta_1^{e_l} & \beta_2^{e_l} & \beta_3^{e_l} & \beta_4^{e_l} \\ \gamma_1^{e_l} & \gamma_2^{e_l} & \gamma_3^{e_l} & \gamma_4^{e_l} \\ \delta_1^{e_l} & \delta_2^{e_l} & \delta_3^{e_l} & \delta_4^{e_l} \end{bmatrix} = \begin{bmatrix} 1 & 0 & 0 & 0 \\ 0 & 1 & 0 & 0 \\ 0 & 0 & 1 & 0 \\ 0 & 0 & 0 & 1 \end{bmatrix},$$

and we can solve for our parameters $\alpha_p^{e_l}, \ldots, \delta_p^{e_l}$ for $p = 1, \ldots, 4$ by matrix inversion. Since our mesh is constant in time, this can be done once prior to the time stepping.

We finally apply Holand-Bell integration to the element vector

$$f_i^{e_l} = \int_{e_l} s_M \mathbb{1}_{Tip} \varphi_i dV = s_M I_{Tip}(e_l) \int_{e_l} \varphi_i dV = \begin{cases} 0 & \text{for } i \notin \{n_p^{e_l} | p = 1, \ldots, 4\} \\ s_M I_{Tip}(e_l) \frac{\|\Delta\|^{e_l}}{144}, & \text{otherwise,} \end{cases}$$

where $I_{Tip}(e_l)$ is a function approximating the percentage of volume of the element e_l taken up by tip cells. For now, we choose this function to be the total volume of the cells with a center inside the tetrahedron divided by the volume of the tetrahedron itself, i.e.

$$I_{Tip}(e_l) = \frac{\sum_{i \in \theta} \frac{4}{3} \pi r_i^3}{\frac{\|\Delta\|^{e_l}}{6}} = \frac{8\pi}{\|\Delta\|^{e_l}} \sum_{i \in \theta} r_i^3,$$

where θ is the set of all tip cells having their center of mass inside the tetrahedron and r_i are there radii. This function does not take into account that cells and tetrahedra can partially overlap. Improvements upon this can be made in the future.

2.4. REST OF THE ELEMENT MATRICES AND VECTORS

Likewise, we derive the elements matrices and vectors for all other equations. We use the same nodal points, hence we have the same basis functions φ_j and the same matrices L. We approximate

$$c_V \approx \sum_{j=1}^{n} c_v(j)\varphi_j, \quad c_D \approx \sum_{j=1}^{n} c_d(j)\varphi_j, \quad c_U \approx \sum_{j=1}^{n} c_u(j)\varphi_j, \quad c_M \approx \sum_{j=1}^{n} c_m(j)\varphi_j,$$
$$c_F \approx \sum_{j=1}^{n} c_f(j)\varphi_j, \quad c_B \approx \sum_{j=1}^{n} c_b(j)\varphi_j, \quad c_E \approx \sum_{j=1}^{n} c_e(j)\varphi_j.$$

We write $M_V^{e_l}, \ldots, M_E^{e_l}$ and $S_V^{e_l}, \ldots, S_E^{e_l}$ for the element matrices and $f_V^{e_l}, \ldots, f_E^{e_l}$ for the element vectors for each variable. Hence we derive systems

$$\sum_{l=1}^{n_{el}} \left(M_V^{e_l}\right) \frac{\partial c_v}{\partial t} + \sum_{l=1}^{n_{el}} \left(S_V^{e_l}\right) c_v = \sum_{l=1}^{n_{el}} f_V^{e_l},$$
$$\vdots$$
$$\sum_{l=1}^{n_{el}} \left(M_E^{e_l}\right) \frac{\partial c_e}{\partial t} + \sum_{l=1}^{n_{el}} \left(S_E^{e_l}\right) c_e = \sum_{l=1}^{n_{el}} f_E^{e_l},$$

2.4.1. ELEMENT MATRICES M^{e_l} FOR THE TIME DERIVATIVE

M^{e_l} is the same for all PDE's

$$M^{e_l} = \frac{\|\Delta\|^{e_l}}{120} \begin{bmatrix} 2 & 1 & 1 & 1 \\ 1 & 2 & 1 & 1 \\ 1 & 1 & 2 & 1 \\ 1 & 1 & 1 & 2 \end{bmatrix}.$$

2.4.2. ELEMENT MATRICES S^{e_l} FOR THE SPACIAL DERIVATIVES

S^{e_l} is different for each PDE.

$$S_V^{e_l} = \frac{\|\Delta\|^{e_l}}{24} \sum_{p=1}^{4} D_V[\rho_f(n_p^{e_l}), \rho_b(n_p^{e_l}), \rho_e(n_p^{e_l})] L^{e_l} (L^{e_l})^T + r_V I_{Tip,Stalk}(e_l) \frac{\|\Delta\|^{e_l}}{720} \begin{bmatrix} 2 & 1 & 1 & 1 \\ 1 & 2 & 1 & 1 \\ 1 & 1 & 2 & 1 \\ 1 & 1 & 1 & 2 \end{bmatrix}.$$

$$S_D^{e_l} = \frac{\|\Delta\|^{e_l}}{24} \sum_{p=1}^{4} D_D[\rho_f(n_p^{e_l}), \rho_b(n_p^{e_l}), \rho_e(n_p^{e_l})] L^{e_l} (L^{e_l})^T + r_D I_{Stalk}(e_l) \frac{\|\Delta\|^{e_l}}{720} \begin{bmatrix} 2 & 1 & 1 & 1 \\ 1 & 2 & 1 & 1 \\ 1 & 1 & 2 & 1 \\ 1 & 1 & 1 & 2 \end{bmatrix}.$$

$$S_U^{e_l} = \frac{\|\Delta\|^{e_l}}{24} \sum_{p=1}^{4} D_U[\rho_f(n_p^{e_l}), \rho_b(n_p^{e_l}), \rho_e(n_p^{e_l})] L^{e_l} (L^{e_l})^T + r_U \frac{\|\Delta\|^{e_l}}{24} \begin{bmatrix} c_f(n_1^{e_l}) & & \emptyset \\ & \ddots & \\ \emptyset & & c_f(n_4^{e_l}) \end{bmatrix}.$$

$$S_M^{e_l} = \frac{\|\Delta\|^{e_l}}{24} \sum_{p=1}^{4} D_M[\rho_f(n_p^{e_l}), \rho_b(n_p^{e_l}), \rho_e(n_p^{e_l})] L^{e_l} (L^{e_l})^T + r_M \frac{\|\Delta\|^{e_l}}{24} \begin{bmatrix} c_b(n_1^{e_l}) & & \emptyset \\ & \ddots & \\ \emptyset & & c_b(n_4^{e_l}) \end{bmatrix}.$$

$$S_F^{e_l} = + r_F \frac{\|\Delta\|^{e_l}}{24} \begin{bmatrix} c_u(n_1^{e_l}) & & \emptyset \\ & \ddots & \\ \emptyset & & c_u(n_4^{e_l}) \end{bmatrix}.$$

$$S_B^{e_l} = + r_B \frac{\|\Delta\|^{e_l}}{24} \begin{bmatrix} c_m(n_1^{e_l}) & & \emptyset \\ & \ddots & \\ \emptyset & & c_m(n_4^{e_l}) \end{bmatrix}.$$

$$S_E^{e_l} = [\emptyset]$$

2.4.3. ELEMENT VECTORS

f^{e_l} is different for all variables

$$f_V^{e_l} = [\emptyset],$$

$$f_D^{e_l} = s_D I_{Tip}(e_l) \frac{\|\Delta\|^{e_l}}{144} \begin{bmatrix} 1 \\ 1 \\ 1 \\ 1 \end{bmatrix},$$

$$f_U^{e_l} = s_U I_{Tip}(e_l) \frac{\|\Delta\|^{e_l}}{144} \begin{bmatrix} 1 \\ 1 \\ 1 \\ 1 \end{bmatrix},$$

$$f_M^{e_l} = s_M I_{Tip}(e_l) \frac{\|\Delta\|^{e_l}}{144} \begin{bmatrix} 1 \\ 1 \\ 1 \\ 1 \end{bmatrix},$$

$$f_F^{e_l} = [\emptyset],$$

$$f_B^{e_l} = [\emptyset],$$

$$f_E^{e_l} = -r_F \frac{\|\Delta\|^{e_l}}{24} \begin{bmatrix} c_u(n_1^{e_l}) & & \emptyset \\ & \ddots & \\ \emptyset & & c_u(n_4^{e_l}) \end{bmatrix} c_f(n_{1,\dots,4}^{e_l}) - r_B \frac{\|\Delta\|^{e_l}}{24} \begin{bmatrix} c_m(n_1^{e_l}) & & \emptyset \\ & \ddots & \\ \emptyset & & c_m(n_4^{e_l}) \end{bmatrix} c_b(n_{1,\dots,4}^{e_l}).$$

2.5. IMPLICIT TIME STEPPING

We now approximate the time derivative for the equation for variable c_m at time step $k+1$ by a Euler backward discretization $\frac{\partial c_m}{\partial t} \approx \frac{c_m^{k+1} - c_m^k}{\Delta t_k}$, for a time step Δt_k, possibly depending on the time step. We begin with the original system

$$M_M \frac{\partial c_m}{\partial t} + S_M c_m = f_M,$$

which is integrated by

$$M_M \frac{c_m^{k+1} - c_m^k}{\Delta t_k} + S c_m^{k+1} = f_M,$$

and gives

$$(M_M + \Delta t_k S_M) c_m^{k+1} = M_M c_m^k + \Delta t_k f_M,$$

and can be rewritten to

$$c_m^{k+1} = (M_M + \Delta t_k S_M)^{-1} (M_M c_m^k + \Delta t_k f_M).$$

We would have liked to conclude that we have derived a fully implicit scheme. However, there are explicit terms coming from the cross terms in the reactive parts in the matrices S and in the vector f_E. Furthermore, the diffusive functions and the indicator functions make the matrices S and the vectors f time dependent. Fortunately, because both M and S are symmetric and non-diagonal, inverting $(M + \Delta t S)$ is not computationally harder than inverting M as we would have to do in the explicit scheme.

We have to take special care when assembling the element vector f_E. We want to maintain conservation of mass and therefore the amount of Fibrin and BM dissolving must be added to the ECL. The amount of fibrin dissolving at timestep $k+1$ in element e_l is equal to

$$r_F \frac{\|\Delta\|^{e_l}}{24} \begin{bmatrix} (c_u(n_1^{e_l}))^k & & \emptyset \\ & \ddots & \\ \emptyset & & (c_u(n_4^{e_l}))^k \end{bmatrix} (\rho_f(n_{1,\dots,4}^{e_l}))^{k+1} = r_F \frac{\|\Delta\|^{e_l}}{24} \begin{bmatrix} (c_u(n_1^{e_l}))^k (\rho_f(n_1^{e_l}))^{k+1} \\ \vdots \\ (c_u(n_4^{e_l}))^k (\rho_f(n_4^{e_l}))^{k+1} \end{bmatrix},$$

and we have a similar relation for the reaction of the BM. This together constitutes for the element vector for the ECF $f_E^{e_l}$:

$$f_E^{e_l} = -r_F \frac{\|\Delta\|^{e_l}}{24} \begin{bmatrix} (c_u(n_1^{e_l}))^k (\rho_f(n_1^{e_l}))^{k+1} \\ \vdots \\ (c_u(n_4^{e_l}))^k (\rho_f(n_4^{e_l}))^{k+1} \end{bmatrix} - r_B \frac{\|\Delta\|^{e_l}}{24} \begin{bmatrix} (c_m(n_1^{e_l}))^k (\rho_b(n_1^{e_l}))^{k+1} \\ \vdots \\ (c_m(n_4^{e_l}))^k (\rho_b(n_4^{e_l}))^{k+1} \end{bmatrix}.$$

Note that the signs change due to the fact that the source terms f_E are on the right hand side of the equation whilst the reactive counterparts are on the left hand side.

2.6. MESHING

For the 3d mesh generation we use an open source application ISO2Mesh created by Fang and Boas [35]. To gain extra computational speed, we use Cuthill-McKee bandwith reduction [36] for our node ordering built into MATLAB by the function `symrcm`.

3

EXPERIMENTING WITH MY OWN CELLULAR POTTS MODEL

As a way of getting acquainted with the existing CPM model by Merks [17], a stripped down version of a CPM mimicking the results by Merks was implemented. This chapter briefly summarizes the choices made in the implementation of this model.

3.1. DIFFERENTIAL EQUATIONS GOVERNING THE CHEMICALS - THE CELLULAR-POTTS CASE

In the *in vitro* situation, we have a fibrin matrix with a homogeneous dissolved concentration of VEGF without cells. We assume that endothelial cells do not secrete any VEGF, and hence there is no need to keep track of the oxygen concentrations, which influence the amount of VEGF secreted.

In analogy to Gamba [10], Serini [11] and Merks [5], the concentration of the chemoattractant VEGF V is governed by the diffusion-reaction PDE

$$\frac{\partial V}{\partial t} = D_V \nabla^2 V - r_V \mathbb{1}_{Tip,Stalk}(x,y) V,$$

where D_V is a diffusive constant, r_V is the reaction speed and $\mathbb{1}(x,y)$ is an indicator function taking value 1 inside the cell and 0 otherwise, i.e.

$$\mathbb{1}(x,y) = \begin{cases} 1 & \text{if } (x,y) \text{ is inside cell}, \\ 0 & \text{otherwise.} \end{cases}$$

Merks uses the Kronecker delta notation $\mathbb{1} = \delta_{\sigma_x,0}$. VEGF diffusion is assumed to be independent of the type of medium it is in. Besides this assumption, VEGF reacts with endothelial cells at a rate that is proportional to the concentration V.

The three enzymes MMP, u-PA and DLL-notch are secreted by tip cells. They diffuse through the tissue. MMP reacts with the boundary membrane to degrade it. u-PA reacts with fibrin to degrade it. DLL-notch binds to nearby endothelial cells to prevent them from becoming tip cells. The governing equations are

$$\begin{array}{lllll} \frac{\partial M}{\partial t} & = D_M \nabla^2 M & - r_M \mathbb{1}_{BM} M & + S_M \mathbb{1}_{Tip}, \\ \frac{\partial U}{\partial t} & = D_U \nabla^2 U & - r_U \mathbb{1}_{Fibrin} U & + S_U \mathbb{1}_{Tip}, \\ \frac{\partial D}{\partial t} & = D_D \nabla^2 D & - r_D \mathbb{1}_{Stalk} D & + S_D \mathbb{1}_{Tip}. \end{array}$$

We model the boundary conditions as "no flux" boundaries. Chemicals can not pass through the boundaries. This is unlike the model uses by Merks [5], where a Dirichlet boundary condition is used "absorbing" the chemoattractant. Merks uses a 500×500 lattice where each site is around $4\mu m^2$ in area. Cells contain around 45 lattice sites, modeling them to have a radius of 7.5 μm.

3.2. STOCHASTIC DEVELOPMENT OF THE SUBSTRATE

The BM degrades into ECM stochastically respectively to the concentration MMP.

Give some mathematical formalisms for this.
Fibrin degrades into ECM stochastically respectively to the concentration u-PA.

Stalk cells are deterministically chosen in the initial distribution of cells.
BM can form stochastically between stalk cells (not tip cells) and either fibrin or the ECM. The concentration MMP should be sufficiently small.

3.3. STOCHASTIC ELONGATION OF THE CELLS

Many studies have been devoted to the dynamics of ECs [1], [37], [38]. We implement the following dynamics. Both tip and stalk cells chemotact towards a gradient of VEGF. Stalk cells also chemotact towards a gradient of DLL-notch.

Cells add lattice sites more easily in ascending order from the BM, Lumen, Fibrin and ECM. Cells never add any lattice sites from the boundary. The Hamiltonian energies are chosen such that this order is attained.

Cells tend to be limit their aspect ratio. Lattice sites in the cell further away from the center of gravity get negative energies.

Cells tend to stick together. Lattice sites directly adjacent to lattice sites in other cells get positive energies.

Cells tend to stick to the BM. Lattice sites directly adjacent to elements in the BM get positive energies.

Cells stay at the same size. Every time step, the most positive and the most negative lattice site in the cell and it's surrounding is calculated and they are acquired and repulsed respectively. This is the largest difference compared to the CPM implemented by Merks.

3.4. MODEL UPDATES

In our computational model, we solve the PDEs on a grid identical to the lattice sites using a finite volumes scheme. Each time step consists of three phases. First, the chemicals are updated. Based on the new distribution of the chemicals, the substrate sites are stochastically degraded. At last, we calculate the maximal and minimal energy lattice site for each cell and acquire and repel the lattice sites successively.

4

POSSIBLE EXTENSIONS TO THE *in vivo* SITUATION

4.1. DIFFERENTIAL EQUATIONS GOVERNING THE CHEMICALS FOR THE *in vivo* SITUATION - THE SEMI-DISCRETE CELL-BASED CASE

In the *in vivo* situation, we have cells contained in the ECM and in between the fibrin that consume oxygen and secrete VEGF when deprived of oxygen. Hence, we additionally have to monitor the oxygen concentrations and this constitutes to a more complex system with more reaction and source terms.

Oxygen sources from the lumen elements at a constant rate and reacts in the fibrin, stalk and tip elements proportional to the concentration. Furthermore, it diffuses and we assume that the diffusion is independent of the type of medium it is in. Hence, we have a diffusion-reaction-source equation governing the concentration of oxygen c_O:

$$\frac{\partial c_O}{\partial t} = D_O \nabla^2 c_O - r_O \mathbb{1}_{Fibrin,Tip,Stalk} c_O + S_O \mathbb{1}_{Lumen},$$

where D_O is the diffusion constant, S_O is the source strength and r_O is the reaction constant.

The cells within the fibrin secrete VEGF reversely proportional to the oxygen concentration. For a certain concentration c_{O_s}, the secretion of VEGF stops. Hence the source strength is proportional to $\max\left(0, 1 - \frac{O}{O_s}\right)$. Furthermore, the VEGF diffuses assuming to be independent of the type of medium it is in. At last, the VEGF reacts with endothelial cells, proportional to the concentration. The diffusion-reaction-source equation governing the concentration of VEGF V looks like:

$$\frac{\partial c_V}{\partial t} = D_V \nabla^2 c_V - r_V \mathbb{1}_{Tip,Stalk} c_V + S_V \max\left(0, 1 - \frac{c_O}{c_{O_s}}\right) \mathbb{1}_{Fibrin},$$

where D_V is the diffusion constant, S_V is the source strength and r_V is the reaction constant.

The three enzymes MMP, u-PA and DLL-notch are secreted by tip cells. They diffuse through the tissue. MMP reacts with the boundary membrane to degrade it. u-PA reacts with fibrin to degrade it. DLL-notch binds to nearby endothelial cells to prevent them from becoming tip cells. The governing equations are

$$\frac{\partial c_M}{\partial t} = D_M \nabla^2 c_M - r_M \mathbb{1}_{BM} c_M + S_M \mathbb{1}_{Tip},$$

$$\frac{\partial c_U}{\partial t} = D_U \nabla^2 c_U - r_U \mathbb{1}_{Fibrin} c_U + S_U \mathbb{1}_{Tip},$$

$$\frac{\partial c_D}{\partial t} = D_D \nabla^2 c_D - r_D \mathbb{1}_{Stalk} c_D + S_D \mathbb{1}_{Tip}.$$

This model to some extent follows the reasoning of Maggelakis in [33].

A

GLOSSARY OF BIOCHEMICAL TERMS AND PROCESSES

A.1. PROCESSES

- *Angiogenesis:* Creation of new blood vessels from pre-existing vessels.
- *Vasculogenesis:* Creation of new blood vessels by forming *endothelial* cells from *mesoderm* cells.
- *Proliferation:* Cell division.
- *Chemotaxis:* Active cell migration in response to a chemical stimulus. Mostly in the direction of the gradient of a concentration field solvent in the surroundings. The substance that cells are being attracted towards is called the *chemoattractant*.
- *Haptotaxis:* Active cell migration in response to a chemical gradient positionally fixed in the *extracellular matrix*. *Fibronectin* is an example of a protein in the basement membrane causing haptotaxis.
- *Elongation:* Changing shape towards an attractant.
- *Contact Inhibition:* A cell not being respondent to autocrine chemotaxis when the membrane is in contact with another cell. For example, *VE-cadherin* which binds cells together causes cells to not respond to *autocrine chemotaxis*.
- *Autocrine Chemotaxis:* Chemotaxis caused by a chemical gradient secreted by the cell itself.
- *Anastomosis:* The process in angiogenesis where sprouts join. Sprouts can join tip-to-tip or the tip cell of a sprout can joint halfway into another sprout.

A.2. PHYSIOLOGICAL DEFINITIONS

- *Endothelial cells:* Cells that line the inside of a blood vessel in a mono-layer. They rest on the *basement membrane*.
- *Endothelium:* The mono-layar of *endothelial cells* forming the inner layer of a blood vessel.
- *HUVECs.* Human Umbilical Vein Endothelial Cells. Endothelial cells acquired from the Umbilical Vein.
- *Motility:* Ability to move and migrate.
- *Mesoderm:* The skin layer between the ectoderm and the endoderm.
- *Fibroblast:* Cells that, among other functions, form the *ECM*.
- *Granulation Tissue:* New connective tissue in the wound healing process that is filled with blood vessels formed by angiogenesis. It is deposited by *fibroblasts*, which rely on oxygen from the blood vessels to do so.

- *ECM:* Extra Cellular Matrix. Everything outside the cells in a multi-cellular structure. Consists of fiber like structures such as *collagen* or *fibrin*. The *Basement membrane* is part of the ECM.
- *Basement membrane:* Thin sheet of fibres beneath the *endothelium*.
- *Hypoxic tissue:* Tissue that is low on oxygen supply. Hypoxic tissue secretes, among other things, *VEGF*.
- *Matrix:* A substance used to grow cell cultures on. Examples are fibrin matrices or Matrigel matrices.
- *Sprout:* Start of a new hair vessel.
- *Tip Cells:* Endothelial cells that are leading the growth of a sprout. Tip cells secrete a signal substance that withholds *stalk cells* to start behaving like tip cells. Tip Cells secrete proteases that degrade the fibrin matrix. The selection of the tip cell is regulated by DLL4 and Notch1. [39]
- *Stalk Cells:* Endothelial cells that follow a tip cell.
- *Lumen:* The space between endothelial cells in which blood can flow.

A.3. SUBSTANCES

- *Angiogenesis inhibitor:* Group of substances that can slow down the process of angiogenesis.
- *Angiogenetic Growth Factors:* Group of substances that can speed up the process of angiogenesis.
- *VEGF:* Vascular Endothelial Growth Factor. An angiogenetic growth factor. A signal protein given off by *hypoxic tissue* to induce angiogenesis. It activates *endothelial cells* in pre-existing blood vessels to degrade the basement membrane.
- *bFGF:* basic Fibroblast Growth Factor, sometimes FGF-2. An angiogenetic growth factor.
- *Collagen:* Structural protein in skin.
- *Fibrin:* Structural protein in skin.
- *VE-cadherin:* A homophilic, trans-membrane cell-adhesion cadherin type protein that binds cells to one another. Besides it's adhesive function, it plays an inhibiting role in the *VEGF* signalling pathway [40]. The contact inhibited chemotaxis is modeled after this effect [17].
- *Proteolytic enzymes:* Enzymes that degenerate proteins.
- *TNFα:* Tumor necrosis factor alpha. Induces receptor bound u-PA (urokinase-type plasminogen activator) activity, a proteolytic enzyme, which degrades fibrin matrices. It is used in fibrin mono layer experiments to maintain the mono-layer.
- *MMP:* matrix metalloproteinase. A proteolytic enzyme secreted by tip cells to degenerate the boundary membrane.
- *u-PA:* urokinase-type plasminogen activator. A proteolytic enzyme secreted by tip cells to degenerate fibrin.
- *VEGF DLL-notch:* Enzyme secreted by tip cells to prevent stalk cells to transform into tip cells and make them chemotactically move towards the tip cell.
- *fibronectin:* a matrix macromolecule which occurs in two distinctly different forms. 1. As a soluble glycoprotein found in various body fluids (including blood), known as plasma fibronectin. 2. As an insoluble constituent of the extracellular matrix and basement membranes of cells, known as cellular fibronectin

BIBLIOGRAPHY

[1] P. Carmeliet *et al.*, *Mechanisms of angiogenesis and arteriogenesis,* Nature medicine **6**, 389 (2000).

[2] H. Rossiter, C. Barresi, J. Pammer, M. Rendl, J. Haigh, E. F. Wagner, and E. Tschachler, *Loss of vascular endothelial growth factor a activity in murine epidermal keratinocytes delays wound healing and inhibits tumor formation,* Cancer research **64**, 3508 (2004).

[3] F. m. c. Graner and J. A. Glazier, *Simulation of biological cell sorting using a two-dimensional extended potts model,* Physical Review Letters **69**, 2013 (1992).

[4] J. A. Glazier and F. Graner, *Simulation of the differential adhesion driven rearrangement of biological cells,* Physical Review E **47**, 2128 (1993).

[5] R. M. Merks, S. A. Newman, and J. A. Glazier, *Cell-oriented modeling of in vitro capillary development,* in *Cellular Automata* (Springer, 2004) pp. 425–434.

[6] R. M. Merks, S. V. Brodsky, M. S. Goligorksy, S. A. Newman, and J. A. Glazier, *Cell elongation is key to in silico replication of in vitro vasculogenesis and subsequent remodeling,* Developments in Biologicals **289**, 44 (2006).

[7] R. M. H. Merks and J. A. Glazier, *Dynamic mechanisms of blood vessel growth,* Nonlinearity **19**, C1 (2006).

[8] F. Vermolen and A. Gefen, *A semi-stochastic cell-based formalism to model the dynamics of migration of cells in colonies,* Biomechanics and modeling in mechanobiology **11**, 183 (2012).

[9] F. Vermolen and O. van Rijn, *A mathematical model for wound contraction and angiogenesis,* (2012).

[10] A. Gamba, D. Ambrosi, A. Coniglio, A. De Candia, S. Di Talia, E. Giraudo, G. Serini, L. Preziosi, and F. Bussolino, *Percolation, morphogenesis, and burgers dynamics in blood vessels formation,* Physical review letters **90**, 118101 (2003).

[11] G. Serini, D. Ambrosi, E. Giraudo, A. Gamba, L. Preziosi, and F. Bussolino, *Modeling the early stages of vascular network assembly,* The EMBO Journal **22**, 1771 (2003).

[12] D. e. a. Horstmann, *From 1970 until present: the keller-segel model in chemotaxis and its consequences,* (2003).

[13] R. B. Vernon and E. H. Sage, *Between molecules and morphology. extracellular matrix and creation of vascular form.* The American journal of pathology **147**, 873 (1995).

[14] P. Namy, J. Ohayon, and P. Tracqui, *Critical conditions for pattern formation and in vitro tubulogenesis driven by cellular traction fields,* Journal of Theoretical Biology **227**, 103 (2004).

[15] D. Manoussaki, S. Lubkin, R. Vemon, and J. Murray, *A mechanical model for the formation of vascular networks in vitro,* Acta Biotheoretica **44**, 271 (1996).

[16] D. Manoussaki, *A mechanochemical model of angiogenesis and vasculogenesis,* ESAIM: Mathematical Modelling and Numerical Analysis **37**, 581 (2003).

[17] R. M. H. Merks, E. D. Perryn, A. Shirinifard, and J. A. Glazier, *Contact-inhibited chemotaxis in de novo and sprouting blood-vessel growth,* PLoS Computational Biology **4**, e1000163 (2008).

[18] A. Gefen, *Effects of virus size and cell stiffness on forces, work, and pressures driving membrane invagination in a receptor-mediated endocytosis,* Journal of biomechanical engineering **132**, 084501 (2010).

[19] N. Chen, J. A. Glazier, J. A. Izaguirre, and M. S. Alber, *A parallel implementation of the cellular potts model for simulation of cell-based morphogenesis,* Computer physics communications **176**, 670 (2007).

[20] F. Vermolen and A. Gefen, *A phenomenological model for chemico-mechanically induced cell shape changes during migration and cell–cell contacts,* Biomechanics and modeling in mechanobiology **12**, 301 (2013).

[21] R. Merkel, N. Kirchgeßner, C. M. Cesa, and B. Hoffmann, *Cell force microscopy on elastic layers of finite thickness,* Biophysical journal **93**, 3314 (2007).

[22] F. Vermolen and A. Gefen, *A semi-stochastic cell-based model for in vitro infected 'wound'healing through motility reduction: A simulation study,* Journal of Theoretical Biology **318**, 68 (2013).

[23] K. L. Johnson and K. L. Johnson, *Contact mechanics* (Cambridge university press, 1987).

[24] T. Alarcón, H. M. Byrne, P. K. Maini, and J. Panovskac, *Mathematical modelling of angiogenesis and vascular adaptation,* Studies in Multidisciplinarity **3**, 369 (2005).

[25] E. Gaffney, K. Pugh, P. Maini, and F. Arnold, *Investigating a simple model of cutaneous wound healing angiogenesis,* Journal of mathematical biology **45**, 337 (2002).

[26] A. R. Anderson and M. Chaplain, *Continuous and discrete mathematical models of tumor-induced angiogenesis,* Bulletin of mathematical biology **60**, 857 (1998).

[27] M. Orme and M. A. Chaplain, *Two-dimensional models of tumour angiogenesis and anti-angiogenesis strategies,* Mathematical Medicine and Biology **14**, 189 (1997).

[28] H. A. Levine, S. Pamuk, B. D. Sleeman, and M. Nilsen-Hamilton, *Mathematical modeling of capillary formation and development in tumor angiogenesis: penetration into the stroma,* Bulletin of mathematical biology **63**, 801 (2001).

[29] F. Vermolen, *Simplified finite-element model for tissue regeneration with angiogenesis,* Journal of engineering mechanics **135**, 450 (2009).

[30] R. C. Schugart, A. Friedman, R. Zhao, and C. K. Sen, *Wound angiogenesis as a function of tissue oxygen tension: a mathematical model,* Proceedings of the National Academy of Sciences **105**, 2628 (2008).

[31] C. Xue, A. Friedman, and C. K. Sen, *A mathematical model of ischemic cutaneous wounds,* Proceedings of the National Academy of Sciences **106**, 16782 (2009).

[32] F. Vermolen and E. Javierre, *A finite-element model for healing of cutaneous wounds combining contraction, angiogenesis and closure,* Journal of mathematical biology **65**, 967 (2012).

[33] S. Maggelakis, *Modeling the role of angiogenesis in epidermal wound healing,* (2003).

[34] I. Holand and K. Bell, *Finite element methods in stress analysis* (Tapir, 1970).

[35] Q. Fang and D. A. Boas, *Tetrahedral mesh generation from volumetric binary and grayscale images,* in *Biomedical Imaging: From Nano to Macro, 2009. ISBI'09. IEEE International Symposium on* (IEEE, 2009) pp. 1142–1145.

[36] E. Cuthill and J. McKee, *Reducing the bandwidth of sparse symmetric matrices,* in *Proceedings of the 1969 24th national conference* (ACM, 1969) pp. 157–172.

[37] L. Coultas, K. Chawengsaksophak, and J. Rossant, *Endothelial cells and vegf in vascular development,* Nature **438**, 937 (2005).

[38] G. Helmlinger, M. Endo, N. Ferrara, L. Hlatky, and R. K. Jain, *Growth factors: formation of endothelial cell networks,* Nature **405**, 139 (2000).

[39] M. Hellström, L.-K. Phng, J. J. Hofmann, E. Wallgard, L. Coultas, P. Lindblom, J. Alva, A.-K. Nilsson, L. Karlsson, N. Gaiano, *et al.*, *Dll4 signalling through notch1 regulates formation of tip cells during angiogenesis,* Nature **445**, 776 (2007).

[40] E. Dejana, *Endothelial cell–cell junctions: happy together,* Nature Reviews Molecular Cell Biology **5**, 261 (2004).